Journal of Biomechanics 54 (2017) 49–57

Contents lists available at ScienceDirect

Journal of Biomechanics

journal homepage: www.elsevier.com/locate/jbiomech
www.JBiomech.com

A transversely isotropic coupled hyperelastic model for the mechanical behavior of tendons

Thiago André Carniel [a], Eduardo Alberto Fancello [a,b,*]

[a] GRANTE - Department of Mechanical Engineering, Universidade Federal de Santa Catarina, Florianópolis, SC, Brazil
[b] LEBm - University Hospital, Universidade Federal de Santa Catarina, Florianópolis, SC, Brazil

ARTICLE INFO

Article history:
Accepted 24 January 2017

Keywords:
Constitutive modeling
Anisotropic
Transversely isotropic
Tendon
Soft tissues

ABSTRACT

Several constitutive models for fibrous soft tissues used in literature provide a completely isotropic response when fibers are compressed. However, recent experimental investigations confirm the expectation that tendons behave anisotropically during compression tests. Motivated by these facts, the present manuscript presents an appropriate choice of hyperelastic potentials able to predict the coupled mechanical behaviors of tendons under both tensile and compressive loads with a relatively small number of material parameters. The high stiffness of tendons under tensile tests is handled by a transversely isotropic model while the coupled compressive response is modeled by means of a Fung-type potential in terms of Seth-Hill's generalized strain tensors. In present study the logarithm strain measure is used instead of the usually employed Green-Lagrange strain. After a parameter identification procedure, the resulting model showed ability to satisfactorily reproduce the experimental data. Details on the analytical material tangent modulus are provided. Present results will then enhance further researches related to tendon dissipative effects and numerical multiscale investigations.

1. Introduction

Tendons are living tissues that react to mechanical loads changing their structure and metabolism. These interactions are issues addressed in mechanotransduction, a branch of mechanobiology that studies the way cells convert mechanical forces into biochemical signals leading to tissue adaptation (Wang, 2006; Lavagnino et al., 2015). Knowing that tenocytes are surrounded by helical collagen fibers (see Section 2), one can realize that even under the usual macroscopic tensile loads along of the direction of the fibers, tendon cells are subjected to complex states of microscopic compressive stresses.

Aiming to the modeling of tendons, a recent experimental investigation has been conducted by Böl et al. (2015) employing semi-confined compression tests on samples at different orientations. The results pointed out quantitatively a behavior that was qualitatively expected: tendons present anisotropy even under compression. Moreover, experimental tests reveal significantly discrepancies in mechanical responses under compressive and tensile states. Volume reduction for both tension and compression has been verified (Böl et al., 2015). In addition, the levels of stress can reach an order of magnitude between compression and tension (compare Figs. 3 and 4, for example). One can argue, under these conditions, that compressive stresses could be disregarded. While this statement is true for some practical purposes, the quantification and proper prediction of these coupled mechanical behaviors at the macroscale will certainly constitute valuable information for a better understanding of the conservative and dissipative mechanisms occurring in smaller scales.

Several constitutive models for fibrous soft tissues found in literature are based on a strain energy composed by two terms attributed to energies stored in the matrix and in the direction of the fibers. While matrix energy contribution is usually described by an isotropic function of strains, that of fibers is expressed by a function of positive values of strains projected in the direction of the fibers (among others, Holzapfel and Gasser, 2001; Chen et al., 2014; Vassoler et al., 2012; Vassoler et al., 2016). Despite their simplicity, these models provide a completely isotropic response when fibers are compressed, which is in contrast to the mentioned experimental evidences. Alternative models that preserve different coupling levels are found in literature (Fung et al., 1979; Holzapfel and Weizsäcker, 1998; Itskov and Aksel, 2004; Freed and Doehring, 2005; Helfenstein et al., 2010).

With this motivation in mind, this manuscript proposes a practical hyperelastic model arrangement and identifies corresponding material parameters suitable to represent the coupled mechanical

* Corresponding author at: GRANTE - Department of Mechanical Engineering, Universidade Federal de Santa Catarina, Florianópolis, SC, Brazil.
E-mail address: eduardo.fancello@ufsc.br (E.A. Fancello).

http://dx.doi.org/10.1016/j.jbiomech.2017.01.042
0021-9290/

behavior of tendons even when submitted to compressive strains. The coupled response is modeled by means of a Fung-type potential in terms of the Seth-Hill's generalized strain tensors, which broadens its well known application. In addition, taking into account that tendons may be subjected to large compressive states, the logarithm strain measure of the Seth-Hill's family is used instead of the usually employed Green-Lagrange strain. The model is aimed to handle the following phenomena: (a) the coupled interaction between the matrix and fibers, experimentally visible in compressive tests and (b) the stiffness in the direction of the fibers (for positive strains) much greater than that found in the direction orthogonal to the fibers. Present work should be considered as an intermediate step for further researches in multiscale modeling of these composite materials.

This manuscript is organized as follows. Section 2 briefly describes the main aspects of morphology and the hierarchical structure of tendinous tissues. Section 3 presents a selected literature review regarding tensile tests, simple shear and semi-confined compression tests on tendons. This experimental information will be necessary to justify the theoretical background and phenomenological modeling developed in Section 4. In order to identify the constitutive material parameters, an optimization strategy is described in Section 5. A set of numerical results are shown in Section 6 and discussed in Section 7, where the relevance of the mechanical coupling is highlighted. Finally, appendices provide the analytical expressions for the stress and the material tangent modulus.

2. Morphology and hierarchical structure of tendons

Tendons are classified as dense regular connective tissues connecting muscles to bones making movement possible. They are capable of transmitting high tensile stresses as well as storing and dissipating energy during mechanical actions (Kierszenbaum and Tres, 2012; Kannus, 2000; Franchi et al., 2007; de Aro et al., 2012; Screen, 2009; Böl et al., 2015). As seen in Fig. 1, tendons are essentially multi-hierarchical structures. Collagen molecules are cross-linked covalently to form collagen fibrils. A bundle of collagen fibrils forms fibers, which in turn are three-dimensionally arranged to form fascicles.

In a "top-down" approach, tendons are surrounded by a loose connective tissue called paratenon, whose mechanical function is to minimize friction forces between tendon and proximal tissues (Franchi et al., 2007). Underneath the paratenon is located a thin sheath of connective tissue referenced to as the epitenon. The epitenon connects fascicles externally, molding the macroscopic structure of tendon. Surrounding the fascicles, a connective tissue called endotenon is found. Also referenced to as the interfascicular matrix (Thorpe et al., 2012), the endotenon coats and binds the fascicles together, where one can find vessels, capillaries and cells (de Aro et al., 2012; Thorpe et al., 2015).

Optical or polarized light micrographs of the longitudinal section of fascicles reveal a wavy or crimp pattern of collagen fibers (Silver et al., 2003; Franchi et al., 2007; Thorpe et al., 2013). This wavy form comes from the helical arrangement of bundles of fibrils (collagen fibers) embedded in a cellular matrix, as can be verified in the recent investigations of Starborg et al. (2013) and Kalson et al. (2015). Moreover, Kalson et al. (2015) provide mean data related to fibril volume fraction and spiral geometry, making it possible to sketch a single collagen fiber, as shown in Fig. 1.

Collagen fibers are constituted by a thee-dimensional arrangement of fibrils embedded in a hydrated proteoglycan-rich matrix, frequently called the ground substance (Kannus, 2000; Provenzano and Vanderby, 2006). It is known that proteoglycans provide tissue hydration due to the hydrophilic properties of its main molecules, the glycosaminoglycans (Yanagishita, 1993; Mouw et al., 2014). In addition, proteoglycans are orthogonally-oriented between fibrils and do not present intra-fibrillar interactions.

Staggered arrays of cross-linked type I collagen molecules and water form fibrils. Collagen fibrils can be considered as the basic structural units of tendons, with an organized and periodic arrangement of collagen molecules, namely D-periodicity (Silver et al., 2003; Buehler, 2006; Franchi et al., 2007; Fratzl, 2008; Svensson et al., 2013; Blanco et al., 2015).

3. Experimental mechanical behavior of tendons

3.1. Simple shear tests

Purslow (2009) investigated the shear behavior of tendons. To assess this property, the initial shear modulus longitudinal and transverse to the direction of the fascicles was measured in three different bovine tendons: calcaneus, superficial digital flexor and deep digital flexor. The results indicated low shear modulus, in both longitudinal and transverse directions, ranging from 2.94 kPa up to 6.38 kPa with no significant differences between longitudinal and transverse directions.

3.2. Semi-confined compression tests

Semi-confined compression tests were conducted by Böl et al. (2015) in cubic samples (4 mm edges) of porcine tendons. The experiments were performed in three distinct compression modes, as illustrated in Fig. 2. In mode I, fascicles are axially compressed. In mode II, fascicles are transversely compressed but allowed to elongate in axial direction. Finally, in mode III, fascicles are transversely compressed and constrained in fascicles (axial) direction. The first Piola-Kirchhoff stress versus stretch curves (mean and standard deviations) related to compression modes are plotted in Fig. 3.

In view of the coordinate axis shown in Fig. 2 and taking into account a homogeneous strain field, the deformation gradient at the end of the tests is,

$$\mathbf{F} = \begin{bmatrix} \lambda_1 & 0 & 0 \\ 0 & \lambda_2 & 0 \\ 0 & 0 & \lambda_3 \end{bmatrix}, \tag{1}$$

where $\lambda_2 = 1.0$ and $\lambda_3 = 0.7$, needing to find λ_1 for each compression mode. Through the experiments, authors provide the volumetric Jacobians at the end of the tests, i.e., $J_{\mathrm{I}} = J_{\mathrm{III}} = 0.88 \pm 0.04$ and $J_{\mathrm{II}} = 0.84 \pm 0.05$. Considering Eq. (1), the volume change is given by $J \overset{\text{def}}{=} \det(\mathbf{F}) = \lambda_1\lambda_2\lambda_3$, resulting in mean values $(\bar{\cdot})$,

$$\begin{cases} \bar{J}_{\mathrm{I}} = \bar{J}_{\mathrm{III}} = 0.88 & \Rightarrow \quad \bar{\lambda}_1^{\mathrm{I}} = \bar{\lambda}_1^{\mathrm{III}} = 1.25714 \\ \bar{J}_{\mathrm{II}} = 0.84 & \Rightarrow \quad \bar{\lambda}_1^{\mathrm{II}} = 1.20 \end{cases}. \tag{2}$$

Despite this, it is reasonable to hypothesize that modes I and III of Bol's test generate a homogeneous strain field (in the sample scale), the results of mode II deserve particular discussion. Due to a compressive stress of just 350 kPa in X_3 direction, the sample reaches a stretch $\bar{\lambda}_1^{\mathrm{II}} = 1.20$, i.e., a positive strain of approximately 20% in the direction of the fibers. This is a huge value if compared with that observed in tensile tests of similar tissues. Fig. 4 displays different experimental stress-stretch curves where stress values of 14 MPa minimum are needed to obtain just 5% of axial strain. Moreover, experimental tensile tests in single tendon fascicles reveal failure at strains of 10% up to 20% (Yamamoto et al., 1999; Robinson et al., 2004; Legerlotz et al., 2010; Svensson et al., 2010; Thorpe et al., 2012). Due to this contrast, it is not clear if

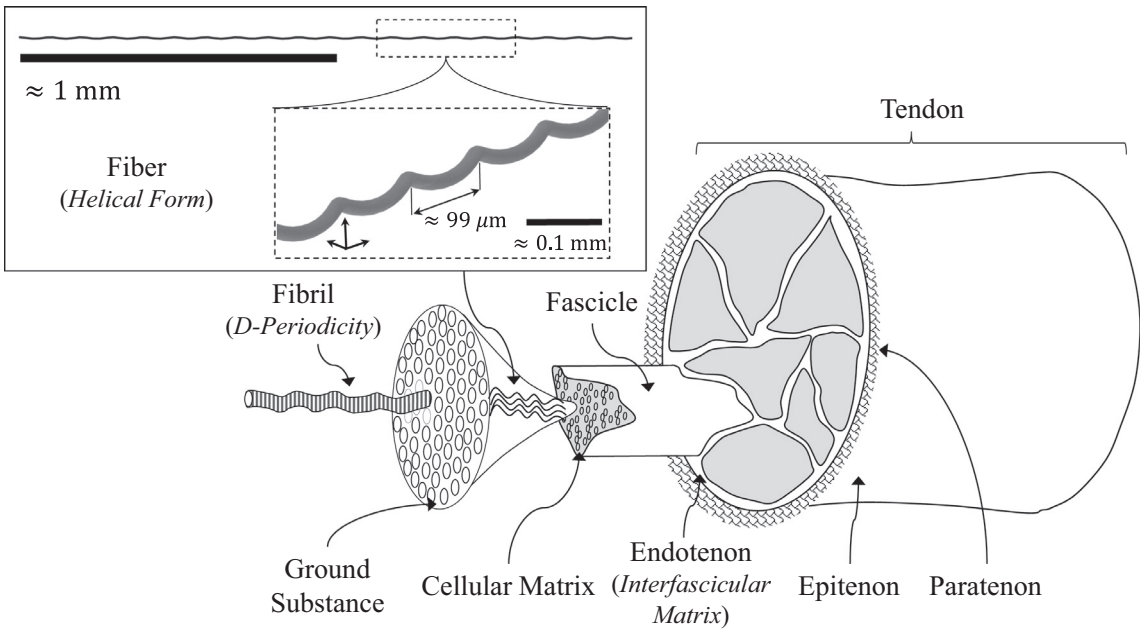

Fig. 1. Illustrative representation of tendons morphology. The inset box shows a sketch of a single collagen fiber in two scales. The data of the helical geometry of the fiber was obtained from Kalson et al. (2015).

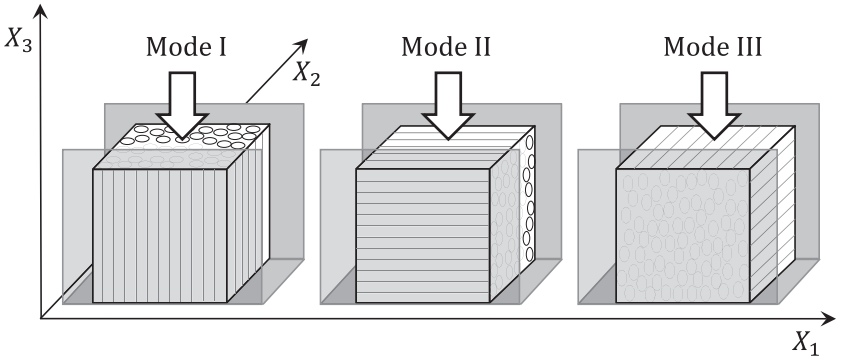

Fig. 2. Illustration of the semi-confined compression tests conducted by Böl et al. (2015).

the homogeneous/mean value $\bar{\lambda}_1^{\mathrm{II}} = 1.20$ experimentally observed in mode II can be equally attributed to both fibers and matrix. In addition, low shear modulus found by Purslow (2009) enhance the significant stiffness difference between collagen structures (fascicles, fibers, fibrils) and their matrices (interfascicular matrix, cellular matrix, ground substance). It is worth mentioning that avoiding sliding among fibers and fascicles is a question of major concern in tensile test protocols, motivating, for example, the use of cryoclamps (Vergari et al., 2011; Thorpe et al., 2012). As a conclusion of these observations, it has been hypothesized that fibers may not be submitted to the observed mean value $\bar{\lambda}_1^{\mathrm{II}}$. Consequently, one can critically question if mode II test yields a homogeneous strain field. Accordingly, the data provided in this mode will not be used in present modeling and corresponding parameters identification.

3.3. Uniaxial tensile tests

Due to the physiological characteristics of tendinous tissues, monotonic tensile tests in the direction of the fibers are the most comprehensive in literature. A short bibliographic survey is synthesized in Table 1, and corresponding stress-stretch curves are plotted in Fig. 4.

Large variations are noted in these curves. Besides technical issues related to experiments, these differences can be assigned to pathological conditions, aging, gender, hormonal disorders, sedentarism, among others (Franchi et al., 2007; Riley, 2008; Magnusson et al., 2010; Arya and Kulig, 2010; de Aro et al., 2012; Nourissat et al., 2015; Couppe et al., 2015). However, regardless of the measurement techniques and protocols, type of tendons and possible pathologies, the characteristic nonlinear shape of all stress-stretch curves remains the same.

4. Phenomenological modeling of tendons

4.1. Proposed model

Following the same general idea of an additive decomposition of the stored strain energy, the Helmholtz function has the form,

$$\psi(\mathbf{C}) \overset{\text{def}}{=} \psi_{m/f}(\mathbf{C}) + \psi_f(I_4), \tag{3}$$

where $\psi_{m/f}$ models the energetic contribution of microstructural interactions between collagen structures and its matrix, while the scalar functional ψ_f represents the strain energy in axial direction of a family of fibers. It is important to state that, different from what

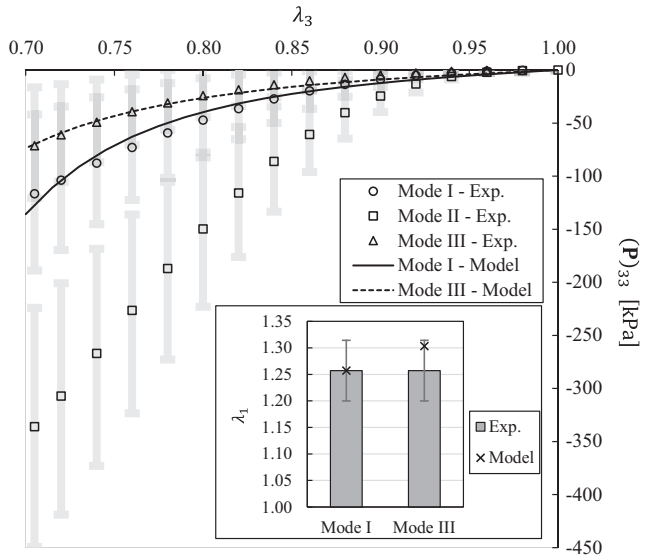

Fig. 3. Comparison between numerical and experimental results obtained from the identification procedure for the semi-confined compression tests conducted by Böl et al. (2015).

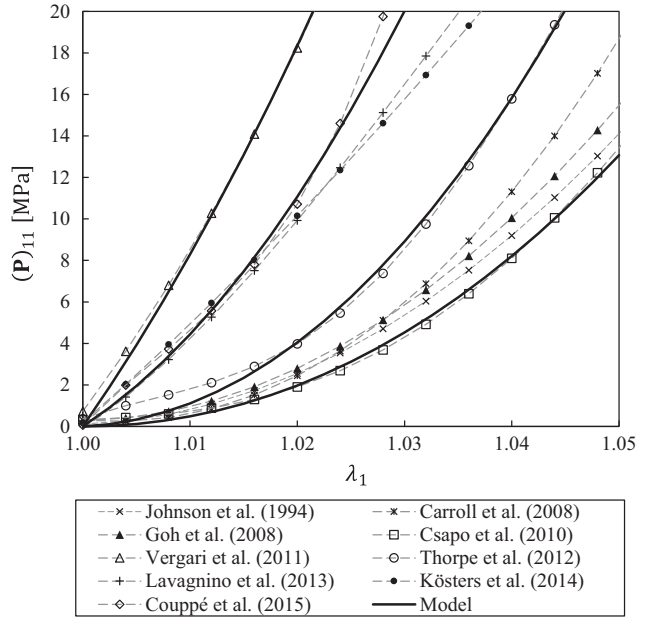

Fig. 4. Monotonic uniaxial tensile test of tendinous tissues. Tendon types and measurement techniques are shown in Table 1. The model parameters and related experimental curves are provided in Table 3.

it seems, this model does not intend to represent a material phase (matrix versus fiber) separation. Both terms of Helmholtz function (3), account for energy accumulated in the fibers and the matrix. However, the additive form was kept because it was observed that this arrangement is a practical way to account for the phenomena herein discussed: (a) the coupled interaction between the matrix and fibers, experimentally visible in compressive tests (controlled by $\psi_{m/f}$), and (b) the stiffness in the direction of the fibers (for positive strains) much greater than that found in the direction orthogonal to the fibers (controlled by ψ_f).

The arguments of Eq. (3) are the right Cauchy-Green strain tensor $\mathbf{C} \stackrel{\text{def}}{=} \mathbf{F}^{\mathrm{T}}\mathbf{F}$ and the invariant,

Table 1
A short bibliographic survey on experimental tensile test of tendons. The related stress-stretch curves are plotted in Fig. 4.

References	Tendon	Strain measurement technique
Johnson et al. (1994)	Human Patellar	DIC
Carroll et al. (2008)	Human Patellar	US
Goh et al. (2008)	Rat Tail	LVDT
Csapo et al. (2010)	Human Achilles	US
Vergari et al. (2011)	Equine Digital Flexor	DIC
Thorpe et al. (2012)	Equine Digital Flexor	DIC
Lavagnino et al. (2013)	Rat Tail	LVDT
Kösters et al. (2014)	Human Patellar	US
Couppe et al. (2015)	Human Achilles	US

DIC – Digital Image Correlation.
US – Ultrasonography.
LVDT – Linear Variable Differential Transformer.

$$I_4 \stackrel{\text{def}}{=} \mathbf{C} : \mathbf{M}_{\mathrm{X}} = \lambda_f^2, \tag{4}$$

in which $\mathbf{M}_{\mathrm{X}} \stackrel{\text{def}}{=} \mathbf{m}_{\mathrm{X}} \otimes \mathbf{m}_{\mathrm{X}}$ is the so called structural tensor, $\mathbf{m}_{\mathrm{X}}$ is a vector representing the directions of the fibers in the reference configuration and λ_f is the stretch in the direction of the fibers.

4.1.1. Transversely isotropic coupled model

Based on the experimental investigations conducted by Purslow (2009) and Böl et al. (2015) (whose results were discussed in Section 3), the free energy $\psi_{m/f}$ is defined as,

$$\psi_{m/f}(\mathbf{C}) \stackrel{\text{def}}{=} \psi_{NH}\left(\hat{\mathbf{C}}\right) + \psi_{Fung}\left(\mathbf{E}_{(n)}\right). \tag{5}$$

Since Purslow's results show that shear behavior of tendons does not change considerably in axial and transverse fiber directions, the strain energy ψ_{NH} is chosen to capture this shear energy by means of an isotropic Neo-Hookean expression:

$$\psi_{NH}\left(\hat{\mathbf{C}}\right) \stackrel{\text{def}}{=} \frac{\mu}{2}\left[\mathrm{tr}\left(\hat{\mathbf{C}}\right) - 3\right]. \tag{6}$$

In Eq. (6), $\mu > 0$ is a material parameter and $\hat{\mathbf{C}} \stackrel{\text{def}}{=} J^{-2/3}\mathbf{C}$ is the isochoric part of the right Cauchy-Green strain tensor. However, as already pointed out, this isotropic energy would be unable to reproduce the semi-confined compression tests of Section 3, and an additional Helmholtz free energy ψ_{Fung} is defined as,

$$\psi_{Fung}\left(\mathbf{E}_{(n)}\right) \stackrel{\text{def}}{=} \frac{C}{2}\left(\mathrm{e}^{Q} - 1\right), \tag{7}$$

which represents a coupled orthotropic model based on the pioneering work of Fung et al. (1979). In Eq. (7), the exponent is given by $Q \stackrel{\text{def}}{=} \mathbf{E}_{(n)} : \mathbb{A} : \mathbf{E}_{(n)}$ and $C > 0$ is a material parameter with unit of stress. The fourth order tensor $\mathbb{A}$ contains the orthotropic parameters and can be mapped in the Voigt notation (underlined tensor variable) as,

$$\underline{\mathbb{A}} \stackrel{\text{def}}{=} \begin{bmatrix} (\mathbb{A})_{1111} & (\mathbb{A})_{1122} & (\mathbb{A})_{1133} & 0 & 0 & 0 \\ & (\mathbb{A})_{2222} & (\mathbb{A})_{2233} & 0 & 0 & 0 \\ & & (\mathbb{A})_{3333} & 0 & 0 & 0 \\ & & & (\mathbb{A})_{1212} & 0 & 0 \\ & \text{sym} & & & (\mathbb{A})_{2323} & 0 \\ & & & & & (\mathbb{A})_{3113} \end{bmatrix}. \tag{8}$$

The second order tensor $\mathbf{E}_{(n)}$ represents a family of Lagrangian strain measures defined by Souza Neto et al. (2009) as,

$$\mathbf{E}_{(n)} \stackrel{\text{def}}{=} \begin{cases} \frac{1}{n}(\mathbf{U}^n - \mathbf{I}) & n \neq 0 \\ \ln(\mathbf{U}) & n = 0 \end{cases}, \tag{9}$$

where n is a real number, $\mathbf{U}$ is the right stretch tensor and $\mathbf{I}$ is the second order identity tensor. As it can be seen from Fig. 1, collagen fibers can be considered straight from the point of view of a macroscopic observer and have a preferential direction into fascicles. Accordingly to this and considering X_1 the direction of fibers and fascicles (see mode II of Fig. 2), it is proposed that the material behavior possesses the following coupling,

$$\begin{cases} (\mathbb{A})_{1111} = c_a \\ (\mathbb{A})_{2222} = (\mathbb{A})_{3333} = c_t \\ (\mathbb{A})_{1122} = (\mathbb{A})_{1133} = c_{at} \\ (\mathbb{A})_{2233} = c_{tt} \\ (\mathbb{A})_{1212} = (\mathbb{A})_{2323} = (\mathbb{A})_{3113} = 0 \end{cases}, \tag{10}$$

where $\{c_a, c_t, c_{at}, c_{tt}\}$are dimensionless material parameters related to the directions of the fibers, i.e., axial, transverse, axial-transverse and transverse-transverse, respectively. It should be noted that shear terms are null, since the corresponding energy is already accounted by ψ_{NH} in (6). Substitution of Eq. (10) into Eq. (8) results in,

$$\underline{\mathbb{A}} = \begin{bmatrix} c_a & c_{at} & c_{at} & 0 & 0 & 0 \\ & c_t & c_{tt} & 0 & 0 & 0 \\ & & c_t & 0 & 0 & 0 \\ & & & 0 & 0 & 0 \\ & \text{sym} & & & 0 & 0 \\ & & & & & 0 \end{bmatrix}, \quad \underline{\mathbb{A}}^* \stackrel{\text{def}}{=} \begin{bmatrix} c_a & c_{at} & c_{at} \\ & c_t & c_{tt} \\ \text{sym} & & c_t \end{bmatrix}, \tag{11}$$

in which is introduced the submatrix $\underline{\mathbb{A}}^* \stackrel{\text{def}}{=} \underline{\mathbb{A}}(1\ldots3, 1\ldots3)$. One can note from Eq. (11) that the orthotropic model reduces to a transversely isotropic one, consistent with the experimental data presented in Section 3.

It is easy to prove that Fung's model (7) is a convex function of $\mathbf{E}_{(n)}$, since it is a non-decreasing, strictly convex function of Q, being that this argument is a quadratic, strictly convex function of $\mathbf{E}_{(n)}$, once the positive semi-definiteness of the fully symmetric tensor $\mathbb{A}$ is guaranteed (Rockafellar, 1970). It should be noted that this property is valid for any symmetric second order strain tensor $\mathbf{E}_{(n)}$. In the present proposition, the positive semi-definiteness of $\mathbb{A}$ is guaranteed if matrix $\underline{\mathbb{A}}^*$ is positive definite, i.e., all its eigenvalues are strictly positive. After some analytical manipulation these requirements yield the following constraints on the material parameters:

$$\mathbf{g} \stackrel{\text{def}}{=} \begin{bmatrix} c_t - c_{tt} \\ 1/2(c_a + c_t + c_{tt}) + B \\ 1/2(c_a + c_t + c_{tt}) - B \end{bmatrix} > \mathbf{0}, \tag{12}$$

with $B = 1/2\sqrt{c_a^2 + c_t^2 + 2(c_t c_{tt} - c_a c_t - c_a c_{tt}) + 8c_{at}^2}$. Guaranteed the convexity of $\psi_{Fung}(\mathbf{E}_{(n)})$, the physical consequences of choosing a specific member of the $\mathbf{E}_{(n)}$ family rely on the ability of the resulting hyperelastic potential to represent the observed physical material behavior. In the material modeling of soft tissues some authors employ the Green-Lagrange strain measure, $\mathbf{E} \stackrel{\text{def}}{=} \mathbf{E}_{(2)}$ (Holzapfel and Weizsäcker, 1998; Holzapfel, 2006; Duong et al., 2015), or even the engineering strain (Rosen et al., 2008) to represent the strain energy (7). However, in the present work, the logarithmic strain measure of Eq. (9) is instead used:

$$\boldsymbol{\varepsilon} \stackrel{\text{def}}{=} \mathbf{E}_{(0)} = \ln(\mathbf{U}) = \frac{1}{2}\ln(\mathbf{C}). \tag{13}$$

The rationale behind this choice is twofold. Firstly, it is well known that for strong compressive stretching states, i.e., for $\lambda \to 0$, engineering and Green's strain converge to finite values (-1.0 and -0.5, respectively) while the logarithmic strain consistently tends to negative infinity. Therefore, this last measure seems to be best suited to soft fibrous tissues, eventually subject to high directional compressive values. Secondly, the logarithmic strain measure provided better results than those of Green's for the parameters identification procedure, as detailed in Section 6.

4.1.2. Unidirectional model

As pointed out in Section 3, the stiffness of tendons under tensile tests is quite high if compared to the stiffness under compression (compare Figs. 3 and 4). Due to this experimental fact, it is proposed that part of the stiffness in the direction of the fibers, i.e., in addition to the component $(\mathbb{A})_{1111}$ of Eq. (8), is activated under tension by means of function ψ_f in Eq. (3). This function is defined as,

$$\psi_f(I_4) \stackrel{\text{def}}{=} \begin{cases} 0 & \text{if} \quad 0 < \lambda_f < 1 \\ k_1(I_4 - 1)^2 + k_2(I_4 - 1)^3 & \text{if} \quad \lambda_f \geqslant 1 \end{cases}, \tag{14}$$

where $k_1 > 0$ and $k_2 > 0$ are material parameters.

Throughout the numerical optimization procedures used to identify the constitutive parameters (Section 5), it has been experienced that the polynomial form defined in Eq. (14) provided quite stable behavior and good representation of experimental data. However, other forms for the strain energy ψ_f, based on the invariant I_4, may be employed, referring to works of Schröder and Neff (2003), Merodio and Ogden (2005), Ehret and Itskov (2007), Holzapfel and Ogden (2009), Helfenstein et al. (2010) and Cheviakov et al. (2015) for further details. The closed forms for the stress and the material tangent modulus are provided in Appendix A.

5. Identification of constitutive parameters

In order to verify if the proposed model is able to represent the observed mechanical responses, an optimization strategy is employed to identify the constitutive parameters. The identification procedure is performed by fitting the results provided by the numerical model to experimental data previously presented in Section 3.

Its important to state that the coupled model (10) was written for a material (tendon) point whose associated local coordinate axis X_1 is aligned with the direction of the fibers. In finite element simulations each integration point must have a local coordinate system aligned with the direction of the fibers, as always required for transversely isotropic materials. Although the knowledge of the direction of the fibers can become a difficult task, the literature points out some experimental and numerical techniques that make this prediction possible and usable in numerical models (Inouye et al., 2015).

5.1. Numerical experiments

The semi-confined tests illustrated in Fig. 2 are assumed to satisfy a homogeneous deformation gradient given by (1). While stretch values (λ_2, λ_3) are a priori defined by the experiment, the axial stretch λ_1 must take a value that satisfies null normal stress on the free faces, i.e., component $(\mathbf{P})_{11}$ of the first Piola-Kirchhoff stress,

$$(\mathbf{P})_{11}(\lambda_1, \lambda_2, \lambda_3) = 0. \tag{15}$$

Since $\lambda_2 = 1.0$ throughout the tests, stretch λ_3 is incremented linearly from 1.0 to 0.7 and λ_1 resulting from the solution of (15) at each time increment.

Uniaxial tensile tests, on the other hand, are set to be controlled by stretch λ_1. Transverse stretches (λ_2, λ_3) must satisfy null values for the transverse first Piola-Kirchhoff stresses:

$$\begin{cases} (\mathbf{P})_{22}(\lambda_1, \lambda_2, \lambda_3) = 0 \\ (\mathbf{P})_{33}(\lambda_1, \lambda_2, \lambda_3) = 0 \end{cases}. \tag{16}$$

5.2. Optimization strategies

Identification of material parameters is an inverse problem usually solved based on a minimization of a cost function defined as the least squared difference between experimental and numerical data:

$$\begin{aligned} &\text{Minimize} \quad f(\mathbf{p}) \\ &\mathbf{p} \in \mathcal{R} \\ &\underline{\mathbf{p}} \leqslant \mathbf{p} \leqslant \overline{\mathbf{p}}, \end{aligned} \tag{17}$$

where $f(\mathbf{p})$ is the objective function, $\mathbf{p}$ is the design vector containing the constitutive parameters, $\underline{\mathbf{p}}$ and $\overline{\mathbf{p}}$ are the lower and upper bounds of the design variables (side constraints) and $\mathcal{R} \stackrel{\text{def}}{=} \{\mathbf{p} | \mathbf{g}(\mathbf{p}) > \mathbf{0}\}$represents the admissible search space constrained by Eqs. (12). It is widely known that the more complex the model, the higher number of experiments are needed to identify the growing number of controlling parameters. Aware that the available experimental data may yield to non-unique parameters corresponding to different local minima, a non-local heuristic algorithm based on Particle Swarm Optimization (PSO) was used to seek for the best global optimizers. Details of this algorithm and its applications in material parameter identification problems are found in Vaz et al. (2013).

Concerning present identification procedure, the strategy proposed is based on two optimization problems. The first one considers the semi-confined compression tests and the second one takes into account the tensile tests. Due to the discussion presented in Section 3.2, only modes I and III are considered throughout the identification procedure for the semi-confined compression tests. For these modes, the energy ψ_f is null (inactive). Moreover, the experimental range of shear modulus, presented in Section 3.1, are set as the lower and upper bounds to shear parameter μ. According to this, only the parameters of model $\psi_{m/f}$ are susceptible to the kinematics imposed by semi-confined compression tests. Therefore, for the first optimization problem, the following objective function is proposed,

$$\begin{aligned} f = \omega_1 f_{\mathbf{P}}\left[(\mathbf{P})_{33}^{\text{Mode I}}\right] + \omega_2 f_{\mathbf{P}}\left[(\mathbf{P})_{33}^{\text{Mode III}}\right] + \omega_3 f_{\lambda}\left(\lambda_1^{\text{Mode I}}\right) \\ + \omega_4 f_{\lambda}\left(\lambda_1^{\text{Mode III}}\right), \end{aligned} \tag{18}$$

where the scalar error function $f_{\lambda}(\cdot) = \left|(\cdot)^{\text{Exp}} - (\cdot)^{\text{Model}}\right|$ and the root mean squared error $f_{\mathbf{P}}(\cdot) = \sqrt{1/N \sum_{i=1}^{N}\left[(\cdot)_i^{\text{Exp}} - (\cdot)_i^{\text{Model}}\right]^2}$ are introduced, and N is the number of points of the stress-stretch curve. The variables $\omega_i, i = 1 \ldots 4$, are weighting factors chosen heuristically in order to prevent one function prevails upon others in the objective function f. The notation $(\cdot)^{\text{Exp}}$ represents the mean value of the experimental data. It is important to notice that through the objective function (18), the optimization algorithm searches for the best set of parameters that minimize, simultaneously, the error of the stress-stretch curves and also the stretch λ_1 at the end of the tests, for both modes I and III.

Once the material parameters $\{\mu, C, c_a, c_t, c_{at}, c_{tt}\}$ of $\psi_{m/f}$ are found, they are fixed and the remaining parameters $\{k_1, k_2\}$of ψ_f seek to reproduce uniaxial tensile stress-stretch curves. This task is performed in the second optimization problem, where the objective function is defined as the root mean squared error of the uniaxial first Piola-Kirchhoff stress curve, i.e., $f = f_{\mathbf{P}}\left[(\mathbf{P})_{11}^{\text{Tensile}}\right]$.

6. Results

The first identification procedure was run considering the experimental data of modes I and III simultaneously. This provided the single set of material parameters shown in Table 2. Using these parameters both modes were simulated and the stress-stretch curves were plotted in Fig. 3. It can then be seen that the model $\psi_{m/f} = \psi_{NH} + \psi_{Fung}$ satisfactorily reproduced the compression curves as well as the stretch values λ_1 (inset bar graph) at the end of the corresponding tests.

It is worth mentioning that the same procedure described above was also performed using the conventional Green's strain measure in the Fung-type model. It was verified that, despite it reproduced equally well the stress-stretch curves, the Green's strain measure was not able to predict transverse λ_1 stretches inside the experimental variations shown in Fig. 3 (convergence to 1.17 and 1.11 for modes I and III, respectively). Moreover, the resulting objective function (18) was approximately 8% larger than that obtained with the logarithmic measure.

Concerning tensile tests, four representative experimental curves were chosen and individually reproduced by the model: lower and upper bounds and two intermediate curves. Corresponding tensile curves are plotted in Fig. 4 and identified parameters sets listed in Table 3. Transverse stretches in all cases were (approximately) $\lambda_2 = \lambda_3 = 0.982$, for a given ultimate axial stretch $\lambda_1 = 1.05$. Taking these results into account and defining uniaxial engineering strain as $\varepsilon_{eng_{(\cdot)}} \stackrel{\text{def}}{=} \lambda_{(\cdot)} - 1$, one can compute the ratio,

$$-\frac{\varepsilon_{eng_2}}{\varepsilon_{eng_1}} = -\frac{\varepsilon_{eng_3}}{\varepsilon_{eng_1}} \approx 0.35. \tag{19}$$

Relation (19) is usually named Poisson's ratio in biomechanical literature. It is worth emphasizing, however, that Poisson is a constant ratio that only applies to isotropic elasticity under linearized kinematics (Böl et al., 2015); once the sample is subject to finite strains, Poisson's ratio loses its strict original physical meaning.

7. Discussions and final remarks

Accordingly to numerical results obtained in compression tests, two points are significant. The first one is related to the fact that mode I is clearly stiffer than mode III (Fig. 3) in spite of the small difference between axial and transverse stiffness parameters c_a and c_t (approximately 1.4%). This different mechanical response should then be attributed to relevant coupling terms c_{at} and c_{tt}. The second remark focuses the transverse-transverse stiffness c_{tt} 16.6% higher than the axial-transverse term c_{at}. This difference points out that significant micromechanisms are activated coupling transverse directions under compressive modes I and III.

As already mentioned, numerical results in tensile tests show the final ratio (19) of ≈ 0.35, which indicates volume augmentation. On the other hand, experimental works of tendon tensile tests in literature frequently report the ratio (19) ranging from 0.55 up to 3 (Lynch et al., 2003; Vergari et al., 2011; Chernak and Thelen, 2012) indicating volume reduction. In this particular case, the model fails to predict the large transverse deformations under tensile tests, since this behavior is modeled by the potential ψ_{Fung}, where corresponding material parameters were firstly identified to reproduce the semi-confined compression tests (see the inset bar graph in Fig. 3).

Some studies refer that these large transverse strains under tensile tests are due to the loss of water during the experiment (Lynch

Table 2
Constitutive parameters related to the numerical curves shown in Fig. 3.

Material model	Parameter	Value	Unit
ψ_{Fung}	C	9.98	kPa
	c_a	14.92	
	c_t	14.70	
	c_{at}	9.64	
	c_{tt}	11.24	
ψ_{NH}	μ	3.76	kPa

Table 3
Material parameters of the unidirectional model ψ_f related to the numerical curves shown in Fig. 4.

Reference	Parameter	
	k_1[MPa]	k_2[MPa]
Csapo et al. (2010)	0.010	197.340
Vergari et al. (2011)	92.779	305.870
Thorpe et al. (2012)	2.893	357.230
Couppe et al. (2015)	42.217	411.360

et al., 2003; Ahmadzadeh et al., 2014; Böl et al., 2015) and biphasic models have been used to account for this observation (Ahmadzadeh et al., 2014; Swedberg et al., 2014). However, understanding in which ways water couples micro-macro behaviors, is still subject to further investigations. Therefore, the formulation of a simple phenomenological model based on continuum mechanics, that is capable to predict these huge differences in the mechanical response of tendons under compression and tension, is a challenge issue in this research field.

Experimental evidences strongly support the theory that tensile loads are mediated mainly by fibrils (Provenzano and Vanderby, 2006; Screen, 2009; Svensson et al., 2011). Although these structures are recognized to present viscous behavior (Shen et al., 2011; Yang et al., 2012), cells and others components of the extracellular matrix, as proteoglycans and water, are pointed out as the main sources of dissipation (Provenzano and Vanderby, 2006; Shen et al., 2011; Connizzo et al., 2013; Kösters et al., 2014). As commented in Section 2, proteoglycans do not present strong interactions with fibrils and are orthogonally-oriented to them. Furthermore, the interstitial fluid flow seems to be directionally dependent (Screen et al., 2011; Ahmadzadeh et al., 2014; Böl et al., 2015). Therefore, due to these micromechanisms and morphologies, viscous effects may have preferential directions throughout tendon hierarchies, which could be reflected macroscopically as anisotropic viscoelastic behavior. Accordingly, the hyperelastic model proposed herein may help future developments in the modeling of dissipative behaviors of tendinous tissues.

8. Conflict of interest statement

The authors have no conflicts of interest.

Acknowledgments

The authors would like to thank the financial support provided by the Brazilian funding agencies CAPES – (Coordination for the Improvement of Higher Education Personnel) and CNPq – (National Council for Scientific and Technological Development).

Appendix A. Stress expressions

From the hyperelastic formalism (Holzapfel, 2000; Bonet and Wood, 2008; Gurtin et al., 2010), the second Piola–Kirchhoff stress tensor is defined as,

$$\mathbf{S} \overset{\text{def}}{=} 2\frac{\partial \psi}{\partial \mathbf{C}}, \tag{A.1}$$

and the first Piola–Kirchhoff stress tensor can be retrieved by $\mathbf{P} \overset{\text{def}}{=} \mathbf{FS}$. In view of (A.1), the derivatives of the Helmholtz free energy (3) result in,

$$\mathbf{S} = \mathbf{S}_{m/f} + \mathbf{S}_f, \quad \mathbf{S}_{m/f} \overset{\text{def}}{=} \mathbf{S}_{NH} + \mathbf{S}_{Fung}, \tag{A.2}$$

where,

$$\mathbf{S}_{NH} = J^{-2/3}\text{dev}_{\mathbf{X}}(\mu \mathbf{I}), \tag{A.3}$$

$$\mathbf{S}_{Fung} = \mathbf{T} : \mathbb{H}, \qquad \mathbf{S}_f = 2\frac{\partial \psi_f}{\partial I_4}\mathbf{M}_{\mathrm{X}}. \tag{A.4}$$

In Eq. (A.3) is introduced the deviatoric operator in the referential configuration $\text{dev}_{\mathbf{X}}(\cdot) \overset{\text{def}}{=} (\cdot) - 1/3[(\cdot) : \mathbf{C}]\mathbf{C}^{-1}$ (Simo, 1998). In view of Eq. (A.4), one can define the derivatives,

$$\mathbf{T} \overset{\text{def}}{=} \frac{\partial \psi_{Fung}}{\partial \boldsymbol{\varepsilon}} = \mathrm{Ce}^{\mathrm{Q}}\mathbb{A} : \boldsymbol{\varepsilon}, \qquad \mathbb{H} \overset{\text{def}}{=} 2\frac{\partial \boldsymbol{\varepsilon}}{\partial \mathbf{C}}, \tag{A.5}$$

and,

$$\frac{\partial \psi_f}{\partial I_4} = \begin{cases} 0 & \text{if} \quad 0 < \lambda_f < 1 \\ 2k_1(I_4 - 1) + 3k_2(I_4 - 1)^2 & \text{if} \quad \lambda_f \geqslant 1 \end{cases}. \tag{A.6}$$

The fourth order tensor $\mathbb{H}$ is evaluated through the derivative of spectral decomposition of $\boldsymbol{\varepsilon}$ in relation to $\mathbf{C}$, whose closed form can be found in Miehe and Lambrecht (2001).

Appendix B. Material tangent modulus

Within the framework of a conventional nonlinear finite element code, the consistent tangent modulus must be provided (Simo and Taylor, 1985). Taking into account a total Lagrangian formulation (Belytschko et al., 2000), the linearization of the equilibrium equations results in the material tangent modulus,

$$\mathbb{C}_{\mathbf{X}} \overset{\text{def}}{=} 2\frac{\partial \mathbf{S}}{\partial \mathbf{C}}. \tag{B.1}$$

The directional derivatives of (A.2), result in the fourth order operators,

$$\mathbb{C}_{\mathbf{X}} = \mathbb{C}_{\mathbf{X}_{m/f}} + \mathbb{C}_{\mathbf{X}_f}, \quad \mathbb{C}_{\mathbf{X}_{m/f}} \overset{\text{def}}{=} \mathbb{C}_{\mathbf{X}_{NH}} + \mathbb{C}_{\mathbf{X}_{Fung}}, \tag{B.2}$$

where,

$$\mathbb{C}_{\mathbf{X}_{NH}} \overset{\text{def}}{=} 2\frac{\partial \mathbf{S}_{NH}}{\partial \mathbf{C}}, \tag{B.3}$$

$$\mathbb{C}_{\mathbf{X}_{Fung}} \overset{\text{def}}{=} \mathbb{H} : \mathbb{E} : \mathbb{H} + \mathbf{T} : \mathbb{L}, \tag{B.4}$$

$$\mathbb{C}_{\mathbf{X}_f} \overset{\text{def}}{=} \left(4\frac{\partial^2 \psi_f}{\partial I_4^2}\right)(\mathbf{M}_{\mathrm{X}} \otimes \mathbf{M}_{\mathrm{X}}). \tag{B.5}$$

The contribution of the Neo-Hookean model (B.3) in the material tangent modulus is well established in literature, and further details can be found in Holzapfel (2000) and Bonet and Wood (2008). Taking into account the operator (B.4), one can define the fourth order tensor,

$$\mathbb{E} \overset{\text{def}}{=} \frac{\partial^2 \psi_{Fung}}{\partial \boldsymbol{\varepsilon} \partial \boldsymbol{\varepsilon}} = \mathrm{Ce}^{\mathrm{Q}}\mathbb{A} + 2\mathrm{Ce}^{\mathrm{Q}}[(\mathbb{A} : \boldsymbol{\varepsilon}) \otimes (\mathbb{A} : \boldsymbol{\varepsilon})], \tag{B.6}$$

and the sixth order tensor $\mathbb{L}$ as,

$$\mathbb{L} \overset{\text{def}}{=} 4\frac{\partial^2 \boldsymbol{\varepsilon}}{\partial \mathbf{C} \partial \mathbf{C}}.$$

Due to the computational costs associated with the calculus of $\mathbb{L}$, the contracted tensor $\mathbf{T} : \mathbb{L}$ is used instead. A closed form for this operation can be found in Miehe and Lambrecht (2001). Finally, the contribution of the unidirectional strain energy ψ_f in the material tangent modulus is expressed as,

$$\frac{\partial^2 \psi_f}{\partial I_4^2} = \begin{cases} 0 & \text{if} \quad 0 < \lambda_f < 1 \\ 2k_1 + 6k_2(I_4 - 1) & \text{if} \quad \lambda_f \geqslant 1 \end{cases}. \tag{B.7}$$

References

Ahmadzadeh, H., Freedman, B.R., Connizzo, B.K., Soslowsky, L.J., Shenoy, V.B., 2014. Micromechanical poroelastic finite element and shear-lag models of tendon predict large strain dependent Poisson's ratios and fluid expulsion under tensile loading. Acta Biomater. 22, 83–91.

Arya, S., Kulig, K., 2010. Tendinopathy alters mechanical and material properties of the Achilles tendon. J. Appl. Physiol. (Bethesda, Md.: 1985) 108 (3), 670–675.

Belytschko, T., Liu, W., Moran, B., 2000. Nonlinear Finite Elements for Continua and Structures. John Wiley & Sons, Ltd.

Blanco, S., Polindara, C.A., Goicolea, J.M., 2015. A regularised continuum damage model based on the mesoscopic scale for soft tissue. Int. J. Solids Struct. 58, 20–33.

Böl, M., Ehret, A.E., Leichsenring, K., Ernst, M., 2015. Tissue-scale anisotropy and compressibility of tendon in semi-confined compression tests. J. Biomech. 48 (6), 1092–1098.

Bonet, J., Wood, R., 2008. Nonlinear continuum mechanics for finite element analysis. Cambridge University Press.

Buehler, M.J., 2006. Nature designs tough collagen: explaining the nanostructure of collagen fibrils. Proc. Natl. Acad. Sci. USA 103, 12285–12290.

Carroll, C.C., Dickinson, J.M., Haus, J.M., Lee, G.A., Hollon, C.J., Aagaard, P., Magnusson, S.P., Trappe, T.a., 2008. Influence of aging on the in vivo properties of human patellar tendon. J. Appl. Physiol. (Bethesda, Md.: 1985) 105 (6), 1907–1915.

Chen, Z., Joli, P., Feng, Z., 2014. Anisotropic hyperelastic behavior of soft biological tissues. Comput. Methods Biomech. Biomed. Eng. (13), 1436–1444

Chernak, L.A., Thelen, D.G., 2012. Tendon motion and strain patterns evaluated with two-dimensional ultrasound elastography. J. Biomech. 45 (15), 2618–2623.

Cheviakov, A.F., Ganghoffer, J.F., St.Jean, S., 2015. Fully non-linear wave models in fiber-reinforced anisotropic incompressible hyperelastic solids. Int. J. Non-Linear Mech. 71, 8–21.

Connizzo, B.K., Yannascoli, S.M., Soslowsky, L.J., 2013. Structure-function relationships of postnatal tendon development: a parallel to healing. Matrix Biol. 32 (2), 106–116.

Couppe, C., Svensson, R.B., Kongsgaard, M., Kovanen, V., Grosset, J.-F., Snorgaard, O., Bencke, J., Larsen, J.O., Bandholm, T., Christensen, T.M., Boesen, A.P., Helmark, I. C., Aagaard, P., Kjaer, M., Magnusson, S.P., 2015. Human Achilles tendon glycation and function in diabetes. J. Appl. Physiol. 9 (23).

Csapo, R., Maganaris, C.N., Seynnes, O.R., Narici, M.V., 2010. On muscle, tendon and high heels. J. Exp. Biol. 213 (Pt 15), 2582–2588.

de Aro, A.A., de Campos Vidal, B., Pimentel, E.R., 2012. Biochemical and anisotropical properties of tendons. Micron 43 (2–3), 205–214.

de Souza Neto, E.A., Peric, D., Owen, D.R.J., 2009. Computational Methods for Plasticity: Theory and Applications.

Duong, M.T., Nguyen, N.H., Staat, M., 2015. Physical response of hyperelastic models for composite materials and soft tissues. Asia Pacific J. Comput. Eng. 2 (3), 1–18.

Ehret, A.E., Itskov, M., 2007. A polyconvex hyperelastic model for fiber-reinforced materials in application to soft tissues. J. Mater. Sci. 42 (21), 8853–8863.

Franchi, M., Trirè, A., Quaranta, M., Orsini, E., Ottani, V., 2007. Collagen structure of tendon relates to function. TheScientificWorldJournal 7, 404–420.

Fratzl, P., 2008. Collagen: structure and mechanics. Springer Science+Business Media.

Freed, A.D., Doehring, T.C., 2005. Elastic model for crimped collagen fibrils. J. Biomech. Eng. 127 (4), 587.

Fung, Y.C., Fronek, K., Patitucci, P., 1979. Pseudoelasticity of arteries and the choice of its mathematical expression. Am. J. Physiol. 237 (5), H620–H631.

Goh, K.L., Holmes, D.F., Lu, H.-Y., Richardson, S., Kadler, K.E., Purslow, P.P., Wess, T.J., 2008. Ageing changes in the tensile properties of tendons: influence of collagen fibril volume fraction. J. Biomech. Eng. 130 (2), 021011.

Gurtin, M., Fried, E., Anand, L., 2010. The mechanics and thermodynamics of continua. Cambridge University Press.

Helfenstein, J., Jabareen, M., Mazza, E., Govindjee, S., 2010. On non-physical response in models for fiber-reinforced hyperelastic materials. Int. J. Solids Struct. 47 (16), 2056–2061.

Holzapfel, G.A., 2000. Nonlinear Solid Mechanics. John Wiley & Sons, Ltd.

Holzapfel, G.A., 2006. Determination of material models for arterial walls from uniaxial extension tests and histological structure. J. Theor. Biol. 238 (2), 290–302.

Holzapfel, G.A., Gasser, T.C., 2001. A viscoelastic model for fiber-reinforced composites at finite strains: continuum basis, computational aspects and applications. Comput. Methods Appl. Mech. Eng. 190 (34), 4379–4403.

Holzapfel, G.A., Ogden, R.W., 2009. Constitutive modelling of passive myocardium: a structurally based framework for material characterization. Philos. Trans. Ser. A, Math. Phys. Eng. Sci. 367 (1902), 3445–3475.

Holzapfel, G.A., Weizsäcker, H.W., 1998. Biomechanical behavior of the arterial wall and its numerical characterization. Comput. Biol. Med. 28 (4), 377–392.

Inouye, J., Handsfield, G., Blemker, S., 2015. Fiber tractography for finite-element modeling of transversely isotropic biological tissues of arbitrary shape using computational fluid dynamics. In: Proceedings of the Conference on Summer Computer Simulation (October 2016), 1–6.

Itskov, M., Aksel, N., 2004. A class of orthotropic and transversely isotropic hyperelastic constitutive models based on a polyconvex strain energy function. Int. J. Solids Struct. 41 (14), 3833–3848.

Johnson, G.A., Tramaglini, D.M., Levine, R.E., Ohno, K., Choi, N.Y., Woo, S.L., 1994. Tensile and viscoelastic properties of human patellar tendon. J. Orthop. Res.: Official Publication Orthop. Res. Soc. 12 (6), 796–803.

Kalson, N.S., Lu, Y., Taylor, S.H., Starborg, T., Holmes, D.F., Kadler, K.E., 2015. A structure-based extracellular matrix expansion mechanism of fibrous tissue growth. eLife 4.

Kannus, P., 2000. Structure of the tendon connective tissue. Scand. J. Med. Sci. Sports 10 (6), 312–320.

Kierszenbaum, A., Tres, L., 2012. Histology and cell biology: an introduction to pathology. Elsevier.

Kösters, A., Wiesinger, H.P., Bojsen-Møller, J., Müller, E., Seynnes, O.R., 2014. Influence of loading rate on patellar tendon mechanical properties in vivo. Clin. Biomech. 29 (3), 323–329.

Lavagnino, M., Gardner, K., Arnoczky, S.P., 2013. Age-related changes in the cellular, mechanical, and contractile properties of rat tail tendons. Connect. Tissue Res. 54 (October 2012), 70–75.

Lavagnino, M., Wall, M.E., Little, D., Banes, A.J., Guilak, F., Arnoczky, S.P., 2015. Tendon mechanobiology: current knowledge and future research opportunities. J. Orthop. Res. 33 (6), 813–822.

Legerlotz, K., Riley, G.P., Screen, H.R.C., 2010. Specimen dimensions influence the measurement of material properties in tendon fascicles. J. Biomech. 43 (12), 2274–2280.

Lynch, H., Johannessen, W., Wu, J., Jawa, A., Elliott, D., 2003. Effect of fiber orientation and strain rate on nonlinear tendon tensile properties. J. Biomech. Eng. 125, 726–731.

Magnusson, S.P., Langberg, H., Kjaer, M., 2010. The pathogenesis of tendinopathy: balancing the response to loading. Nat. Rev. Rheumatol. 6 (5), 262–268.

Merodio, J., Ogden, R.W., 2005. Mechanical response of fiber-reinforced incompressible non-linearly elastic solids. Int. J. Non-Linear Mech. 40 (2–3), 213–227.

Miehe, C., Lambrecht, M., 2001. Algorithms for computation of stresses and elasticity moduli in terms of Seth-Hill's family of generalized strain tensors. Commun. Numer. Methods Eng. 17 (5), 337–353.

Mouw, J.K., Ou, G., Weaver, V.M., 2014. Extracellular matrix assembly: a multiscale deconstruction. Nat. Rev. Molec. Cell Biol. 15 (12), 771–785.

Nourissat, G., Berenbaum, F., Duprez, D., 2015. Tendon injury: from biology to tendon repair. Nat. Publish. Group 11 (4), 1–11.

Provenzano, P.P., Vanderby, R., 2006. Collagen fibril morphology and organization: implications for force transmission in ligament and tendon. Matrix Biol. 25 (2), 71–84.

Purslow, P.P., 2009. The shear modulus of connections between tendon fascicles. In: TIC-STH'09: 2009 IEEE Toronto International Conference – Science and Technology for Humanity, pp. 134–136.

Riley, G., 2008. Tendinopathy-from basic science to treatment. Nat. Clin. Pract. Rheumatol. 4 (2), 82–89.

Robinson, P.S., Lin, T.W., Reynolds, P.R., Derwin, K.a., Iozzo, R.V., Soslowsky, L.J., 2004. Strain-rate sensitive mechanical properties of tendon fascicles from mice with genetically engineered alterations in collagen and decorin. J. Biomech. Eng. 126 (2), 252–257.

Rockafellar, R., 1970. Convex Analysis. Princeton University Press.

Rosen, J., Brown, J.D., De, S., Sinanan, M., Hannaford, B., 2008. Biomechanical properties of abdominal organs in vivo and postmortem under compression loads. J. Biomech. Eng. 130 (2), 021020.

Schröder, J., Neff, P., 2003. Invariant formulation of hyperelastic transverse isotropy based on polyconvex free energy functions. Int. J. Solids Struct. 40 (2), 401–445.

Screen, H.R., 2009. Hierarchical approaches to understanding tendon mechanics. J. Biomech. Sci. Eng. 4 (4), 481–499.

Screen, H.R.C., Seto, J., Krauss, S., Boesecke, P., Gupta, H.S., 2011. Extrafibrillar diffusion and intrafibrillar swelling at the nanoscale are associated with stress relaxation in the soft collagenous matrix tissue of tendons. Soft Matter 7 (23), 11243–11251.

Shen, Z.L., Kahn, H., Ballarini, R., Eppell, S.J., 2011. Viscoelastic properties of isolated collagen fibrils. Biophys. J. 100 (12), 3008–3015.

Silver, F.H., Freeman, J.W., Seehra, G.P., 2003. Collagen self-assembly and the development of tendon mechanical properties. J. Biomech. 36 (10), 1529–1553.

Simo, J., 1998. Numerical analysis and simulation of plasticity. Handbook of Numerical Analysis VI (Part 3).

Simo, J., Taylor, R., 1985. Consistent tangent operators for rate-independent elastoplasticity. Comput. Methods Appl. Mech. Eng. 48 (1), 101–118.

Starborg, T., Kalson, N.S., Lu, Y., Mironov, A., Cootes, T.F., Holmes, D.F., Kadler, K.E., 2013. Using transmission electron microscopy and 3View to determine collagen fibril size and three-dimensional organization. Nat. Protocols 8 (7), 1433–1448.

Svensson, R.B., Hassenkam, T., Grant, C.A., Magnusson, S.P., 2010. Tensile properties of human collagen fibrils and fascicles are insensitive to environmental salts. Biophys. J. 99 (12), 4020–4027.
Svensson, R.B., Hassenkam, T., Hansen, P., Kjaer, M., Magnusson, S.P., 2011. Tensile force transmission in human patellar tendon fascicles is not mediated by glycosaminoglycans. Connect. Tissue Res. 52 (December 2010), 415–421.
Svensson, R.B., Mulder, H., Kovanen, V., Magnusson, S.P., 2013. Fracture mechanics of collagen fibrils: influence of natural cross-links. Biophys. J. 104 (11), 2476–2484.
Swedberg, A.M., Reese, S.P., Maas, S.A., Ellis, B.J., Weiss, J.A., 2014. Continuum description of the Poisson's ratio of ligament and tendon under finite deformation. J. Biomech. 47 (12), 3201–3209.
Thorpe, C.T., Birch, H.L., Clegg, P.D., Screen, H.R.C., 2013. The role of the non-collagenous matrix in tendon function. Int. J. Exp. Pathol. 94 (4), 248–259.
Thorpe, C.T., Birch, H.L., Clegg, P.D., Screen, H.R.C., 2015. Tendon physiology and mechanical behavior: structure-function relationships. In: Gomes, M., Reis, R., Rodrigues, M. (Eds.), Tendon Regeneration: Understanding Tissue Physiology and Development to Engineer Functional Substitutes. Elsevier Academic Press, pp. 3–39 (Chapter 1).
Thorpe, C.T., Udeze, C.P., Birch, H.L., Clegg, P.D., Screen, H.R.C., 2012. Specialization of tendon mechanical properties results from interfascicular differences. J. Roy. Soc. Interface 9 (July), 3108–3117.
Vassoler, J.M., Reips, L., Fancello, E.A., 2012. A variational framework for fiber-reinforced viscoelastic soft tissues. Int. J. Numer. Methods Eng. 89 (13), 1691–1706.
Vassoler, J.M., Stainier, L., Fancello, E.A., 2016. A variational framework for fiber-reinforced viscoelastic soft tissues including damage. Int. J. Numer. Methods Eng.
Vaz Jr., M., Cardoso, E.L., Stahlschmidt, J., 2013. Particle swarm optimization and identification of inelastic material parameters. Eng. Comput. 30 (7), 936–960.
Vergari, C., Pourcelot, P., Holden, L., Ravary-Plumioën, B., Gerard, G., Laugier, P., Mitton, D., Crevier-Denoix, N., 2011. True stress and Poisson's ratio of tendons during loading. J. Biomech. 44 (4), 719–724.
Wang, J.H.C., 2006. Mechanobiology of tendon. J. Biomech. 39 (9), 1563–1582.
Yamamoto, E., Hayashi, K., Yamamoto, N., 1999. Mechanical properties of collagen fascicles from the rabbit patellar tendon. J. Biomech. Eng. 121 (1), 124–131.
Yanagishita, M., 1993. Function of proteoglycans in the extracellular matrix. Acta Pathol. Japonica 43 (3), 283–293.
Yang, L., van der Werf, K.O., Dijkstra, P.J., Feijen, J., Bennink, M.L., 2012. Micromechanical analysis of native and cross-linked collagen type I fibrils supports the existence of microfibrils. J. Mech. Behav. Biomed. Mater. 6, 148–158.